PROCEEDINGS OF SCIENCE

Higgs Pair Production in the 2HDM: Impact of Loop Corrections to the Trilinear Higgs couplings

S. Heinemeyer*
Instituto de Física Teórica (UAM/CSIC), Universidad Autónoma de Madrid, Cantoblanco, 28049, Madrid, Spain
E-mail: Sven.Heinemeyer@cern.ch

M. Mühlleitner
Institute for Theoretical Physics, Karlsruhe Institute of Technology, 76128 Karlsruhe, Germany
E-mail: margarete.muehlleitner@kit.edu

K. Radchenko
Deutsches Elektronen-Synchrotron DESY, Notkestr. 85, 22607 Hamburg, Germany
E-mail: kateryna.radchenko@desy.de

G. Weiglein
Deutsches Elektronen-Synchrotron DESY, Notkestr. 85, 22607 Hamburg, Germany
II. Institut für Theoretische Physik, Universität Hamburg, Luruper Chaussee 149, 22761 Hamburg, Germany
E-mail: georg.weiglein@desy.de

We review the impact of potentially large higher-order corrections on trilinear Higgs couplings (THCs) on the comparison between the experimental results and the theoretical predictions for the pair production of the 125 GeV Higgs boson at the LHC. We use the theoretical framework of the Two Higgs Doublet Model (2HDM), containing besides the SM-like CP-even Higgs boson h a second CP-even Higgs boson H, which we assume to be heavier, $m_H > m_h$. Concerning the invariant mass distribution of the two produced Higgs bosons we demonstrate that the loop corrections to the THCs λ_{hhh} and λ_{hhH} as well as interference contributions give rise to important effects both for the differential and the total cross section. We discuss the implications for the experimental limits that can be obtained in the 2HDM.

Loops and Legs in Quantum Field Theory (LL2024)
14-19, April, 2024
Wittenberg, Germany

*Speaker.

PoS(LL2024)027

1. Introduction

After the discovery of a new scalar particle with a mass of about 125 GeV by ATLAS and CMS in 2012, the determination of its triple Higgs coupling (THC) is now in the focus particle physics, both from the experimental as well as from the theory side. On the other hand, scalar particles play a fundamental role in the proposed answers to several open issues of the Standard Model (SM). Among the most prominent shortcomings of the SM is its inability to explain the observed baryon asymmetry of the universe (BAU). A dynamical explanation is given by electroweak baryogenesis (EWBG), requiering a strong first order EW phase transition (SFOEWPT). While no conclusive sign of BSM physics has been discovered so far, extended scalar sectors, featuring parameter regions that are in agreement with all experimental and theoretical constraints, are particularly appealing in this context. An SFOEWPT related to a shift in the prediction for λ_{hhh} can generically occur in models with extended Higgs sectors via the higher-order corrections involving additional heavy states [1, 2]. It has been demonstrated that in simple extensions such as the Two Higgs Doublet Model (2HDM) the loop corrections to λ_{hhh} can change the tree-level value by several 100% while being in agreement with all existing experimental and theoretical constraints [1, 3].

We define κ_λ as the coupling modifier relative to the tree-level THC in the SM,

$$\kappa_\lambda \equiv \frac{\lambda_{hhh}}{\lambda_{\rm SM}^{(0)}}\,, \quad \text{with} \quad \lambda_{\rm SM}^{(0)} = \frac{m_h^2}{2v^2} \simeq 0.13\,. \tag{1.1}$$

The Large Hadron Collider in its High Luminosity phase (HL-LHC) will be able to significantly improve the sensitivity to possible effects in κ_λ in BSM scenarios [4]. Current prospects for the sensitivity at the HL-LHC with $3\,\text{ab}^{-1}$ integrated luminosity per detector are $-0.5 < \kappa_\lambda < 1.6$ at the 1σ level in the combination of the $b\bar{b}b\bar{b}$, $b\bar{b}\gamma\gamma$ and $b\bar{b}\tau^+\tau^-$ channels [5]. This on the one hand motivates precise theoretical predictions for the Higgs pair production process, which at the (HL-) LHC is dominantly given by gluon fusion into Higgs pairs, taking into account the possibility of sizable BSM contributions to the occurring trilinear Higgs couplings. On the other hand it is important to ensure that the obtained experimental bounds on the gluon fusion Higgs pair production process can be confronted in a meaningful way with theoretical predictions in different scenarios of electroweak symmetry breaking, where a resonant contribution from the exchange of a heavy neutral Higgs boson might be possible in addition to the non-resonant contributions that are always present. The latter contain in particular a contribution involving the Higgs boson at 125 GeV and a top-loop induced contribution where no resonant Higgs boson enters at leading order.

Here we use the well motivated 2HDM as theoretical framework, but it should be stressed that our qualitative results are applicable to a wide class of extended Higgs sectors. Our results are based on Ref. [6]. We review the effects of two contributions entering the process of gluon fusion into Higgs pairs, $gg \to hh$, which provides direct access to λ_{hhh} at the LHC. In particular, we review the effect of potentially large higher-order corrections to λ_{hhh} and λ_{hhH} on the Higgs pair production process. It is demonstrated that the combination of the two effects has important implications on the experimental limits that can be extracted from the Higgs pair production process.

2. Higgs Pair Production in the 2HDM

2.1 The 2HDM and its THCs

Here we briefly review the main definitions. More details can be found in Ref. [6]. We assume a CP-conserving 2HDM (see Ref. [7] for a review). The two Higgs doublets Φ_1 and Φ_2 can be conveniently parametrized as

$$\Phi_1 = \begin{pmatrix} \phi_1^+ \\ \frac{1}{\sqrt{2}}(v_1+\rho_1+i\eta_1) \end{pmatrix}, \qquad \Phi_2 = \begin{pmatrix} \phi_2^+ \\ \frac{1}{\sqrt{2}}(v_2+\rho_2+i\eta_2) \end{pmatrix}, \tag{2.1}$$

in terms of their respective vacuum expectation values, v_1 and v_2 (with $\sqrt{v_1^2+v_2^2} \equiv v \approx 246\,\text{GeV}$), and the interaction fields $\phi_{1,2}^\pm$, $\rho_{1,2}$ and $\eta_{1,2}$ that mix to give rise to five physical scalar fields and three (would-be) Goldstone bosons. The physical fields comprise two CP-even fields, h and H, where by convention $m_h < m_H$, and we identify h with the scalar boson observed at the LHC at about 125 GeV, one CP-odd field, A, and one charged Higgs pair, $H^\pm$. The mixing matrices diagonalizing the CP-even and CP-odd/charged Higgs mass matrices can be expressed in terms of the mixing angles α and β, respectively, with $\tan\beta \equiv v_2/v_1$.

The occurrence of tree-level flavor-changing neutral currents (FCNC) is avoided by extending a $\mathbb{Z}_2$ symmetry from the Higgs sector ($\Phi_1 \to \Phi_1$, $\Phi_2 \to -\Phi_2$) to the Yukawa sector. This results in four variants of the 2HDM, depending on the $\mathbb{Z}_2$ parities of the fermion types. Here we focus on the Yukawa type I, where all fermions couple to Φ_2. The couplings of the neutral CP-even Higgs bosons to fermions are given by $\mathscr{L} = -\sum_{f=u,d,l} \frac{m_f}{v}\left[\xi_h^f \bar{f} f h + \xi_H^f \bar{f} f H\right]$, where m_f are the fermion masses, and $\xi_{h,H}^f$ are the fermionic Yukawa coupling modifiers, which express the couplings relative to the ones of the SM Higgs. In the type I 2HDM the coupling modifiers are equal for all fermions and given by $\xi_h^f = s_{\beta-\alpha} + c_{\beta-\alpha}\cot\beta$, $\xi_H^f = c_{\beta-\alpha} - s_{\beta-\alpha}\cot\beta$ $(f = t,b,\tau)$. We work in the physical basis of the 2HDM, where the Higgs potential parameters are expressed in terms of a set of parameters given mostly by physical quantities as

$$c_{\beta-\alpha},\ t_\beta,\ v,\ m_h,\ m_H,\ m_A,\ m_{H^\pm},\ m_{12}^2. \tag{2.2}$$

Here, $m_h, m_H, m_A, m_{H^\pm}$ are the masses of the physical scalars, m_{12}^2 breaks softly the $\mathbb{Z}_2$ symmetry in the Higgs potential, and we use the short-hand notation $s_x \equiv \sin x$, $c_x \equiv \cos x, t_\beta \equiv \tan\beta$.

The generic tree-level THCs $\lambda^{(0)}_{hh_ih_j}$ involving at least one Higgs boson h with $m_h \sim 125$ GeV are defined such that the Feynman rules are given by $-ivn!\lambda^{(0)}_{hh_ih_j}$, where n is the number of identical particles in the vertex. The 2HDM tree-level THCs $\lambda^{(0)}_{hhh}$ and $\lambda^{(0)}_{hhH}$ can be cast into the forms

$$\lambda^{(0)}_{hhh} = \frac{1}{2v^2}\left\{ m_h^2 s^3_{\beta-\alpha} + \left(3m_h^2 - 2\bar{m}^2\right) c^2_{\beta-\alpha} s_{\beta-\alpha} + 2\cot 2\beta \left(m_h^2 - \bar{m}^2\right) c^3_{\beta-\alpha} \right\}, \tag{2.3}$$

$$\begin{aligned} \lambda^{(0)}_{hhH} = -\frac{c_{\beta-\alpha}}{2v^2}\Big\{ & \left(2m_h^2 + m_H^2 - 4\bar{m}^2\right) s^2_{\beta-\alpha} + 2\cot 2\beta \left(2m_h^2 + m_H^2 - 3\bar{m}^2\right) s_{\beta-\alpha} c_{\beta-\alpha} \\ & - \left(2m_h^2 + m_H^2 - 2\bar{m}^2\right) c^2_{\beta-\alpha} \Big\}, \quad \text{with} \quad \bar{m}^2 = \frac{m_{12}^2}{s_\beta c_\beta}. \end{aligned} \tag{2.4}$$

In the 2HDM, it has been shown that the loop contributions to the THCs involving the heavy BSM Higgs bosons can give rise to corrections of the order of 100% and larger [1, 8] w.r.t. their tree-level values. More recently, also two-loop corrections have been computed [9], potentially enhancing the one-loop effects. For the computation of the one-loop corrections to the THCs contributing to our numerical analysis we use the public code `BSMPT` [10–12], where the trilinear Higgs couplings are extracted from the one-loop corrected effective potential (evaluated here at zero temperature),

$$V_{\rm eff} = V_{\rm tree} + V_{\rm CW} + V_{\rm CT} \,. \tag{2.5}$$

In this equation, $V_{\rm tree}$ is the tree-level potential of the 2HDM, $V_{\rm CW}$ is the one-loop Coleman–Weinberg potential [13, 14] at zero temperature, and $V_{\rm CT}$ is the counterterm potential. The counterterm potential is chosen such that the masses and mixing angles are kept at their tree-level values.

2.2 Di-Higgs production in the 2HDM at the LHC

The THCs are directly accessible in Higgs pair production. At the LHC, the dominant process is gluon fusion into Higgs pairs, which at leading order is mediated by heavy quark loops, see Fig. 1. The THCs enter through the s-channel diagrams, as shown in the first two diagrams of Fig. 1.

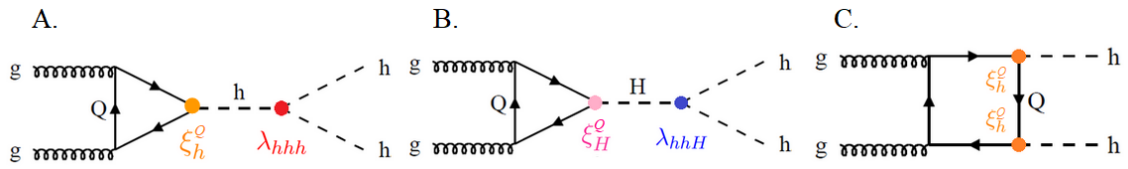

Figure 1: Generic diagrams contributing to the pair production of the Higgs boson h at about 125 GeV in gluon fusion within the 2HDM, mediated by heavy quark loops, $Q = t, b$. The red and blue dots denote the triple Higgs couplings λ_{hhh} and λ_{hhH}, respectively, evaluated at leading or next-to-leading order; the orange (pink) dot denotes the h (H) Yukawa coupling parametrized by the coupling modifier ξ_h^Q (ξ_H^Q). The diagrams labelled as A and C are the continuum diagrams, which appear in analogous form in the SM. The diagram labelled B is the resonant diagram, involving the s-channel heavy H exchange.

In the 2HDM, there are two potential sources of changes w.r.t. the SM. Firstly, the couplings in the SM-like diagrams can differ from the SM values. As discussed above, this applies particularly to λ_{hhh}. Changes in this THC can modify the interference of the SM-like triangle and box diagrams. Secondly, there is an additional s-channel contribution from the heavy Higgs boson, involving the trilinear coupling λ_{hhH} and the top Yukwawa coupling of the H. In case the mass m_H exceeds twice the mass of the lighter Higgs boson, $m_H > 2m_h \sim 250\,\text{GeV}$, this contribution can lead to resonant hh production, in which case the corresponding diagram is referred to as "resonant diagram". Thereby, the cross section can be significantly enhanced. On the other hand, there can also be destructive interferences between the triangle diagrams of the h and H exchange and the box diagram. Accordingly, the loop contributions to the trilinear Higgs couplings are expected to have an important impact both on the prediction for the inclusive cross section and also for the shape of the invariant mass distributions. In Ref. [6] we included for the first time in the 2HDM

the one-loop corrections to the triple Higgs couplings in the computation of Higgs pair production and analyzed their effects.[1]

For the numerical evaluation, we used the code HPAIR [16–19], adapted to the 2HDM. The calculations are carried out at leading order (LO) with the full top-quark mass dependence and (where indicated) include NLO QCD corrections, assuming the limit of an infinite top-quark mass and neglecting bottom loop contributions. Furthermore, for this analysis, we have modified HPAIR to include effective one-loop corrections to the THCs as described above.

3. Impact of loop corrections to THCs on m_{hh}

Here we review the behavior of the invariant mass distribution of the di-Higgs final state when incorporating loop corrections to the THCs involved in Higgs pair production. In Fig. 2 we present various m_{hh} distributions for a sample benchmark point in the 2HDM of type I. It is defined by the input parameters

$$\begin{gathered} t_\beta = 10,\ c_{\beta-\alpha} = 0.13\ (s_{\beta-\alpha} > 0) \\ m_H = 465\ \text{GeV},\ m_A = m_{H^\pm} = 660\ \text{GeV} \ \text{ and } m_{12}^2 = m_H^2 c_\alpha^2 / t_\beta . \end{gathered} \tag{3.1}$$

For this point we find

$$\kappa_\lambda^{(0)} \equiv \frac{\lambda_{hhh}^{(0)}}{\lambda_{\text{SM}}^{(0)}} = 0.84,\ \kappa_\lambda^{(1)} \equiv \frac{\lambda_{hhh}^{(1)}}{\lambda_{\text{SM}}^{(0)}} = 3.65,\ \lambda_{hhH}^{(0)} = 0.10 \text{ and } \lambda_{hhH}^{(1)} = 0.25. \tag{3.2}$$

The THC of the SM-like Higgs boson is hence very SM-like at tree level, but substantially increased by one-loop corrections. The THC between the heavy Higgs boson and the two light Higgs bosons is roughly doubled by the one-loop corrections.

Concerning the invariant mass distributions shown in our analysis, it is important to note that they are calculated at leading order. It would be possible to compute the invariant mass spectrum with HPAIR at NLO QCD in the Born improved heavy-top limit, but mass effects are know to significantly modify the shape of the m_{hh} distribution []. Since no public code is available that includes the full top mass dependence, in particular including resonances, we chose to fully neglect the NLO QCD effects.

We start with the left plot of Fig. 2, showing the m_{hh} distributions without experimental uncertainties. The blue curve is the invariant mass distribution for the specified benchmark point with both THCs taken at tree-level, whereas the red line displays the result for the distribution for the case where both THCs are incorporated at the one-loop level. The dashed black line indicates the SM prediction. Starting our discussion with the tree-level distribution (blue line), several features can be noticed. The small values of the differential cross section just above the threshold are a consequence of a cancellation of the form factors involved in the continuum diagrams (diagrams A and C in Fig. 1). The invariant mass distribution reaches a maximum at $m_{hh} \approx 400$ GeV, which is related to the di-top on-shell production and is also present in the distribution of single Higgs production. A further striking feature is the resonance located at $m_{hh} \approx m_H$ showing a peak-dip

[1] For the SM di-Higgs production, this type of one-loop corrections was discussed in [15].

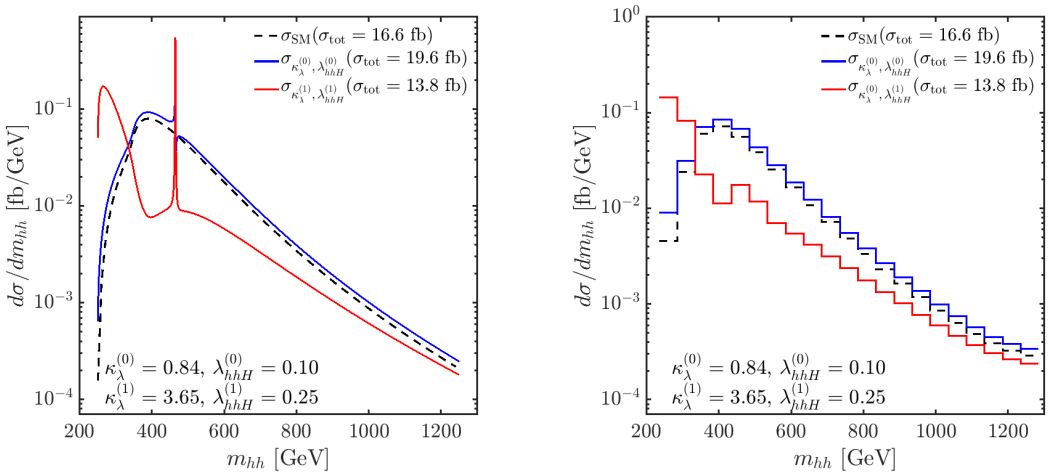

Figure 2: Invariant mass distribution for the benchmark point in the 2HDM type I defined in Eq. (3.1). The SM prediction (dashed black line) is shown together with the 2HDM results with and without loop corrections to the THCs, see text. Left plot: without experimental uncertainties; right plot: including 15% smearing and 50 GeV binning (see text). Left plot taken from Ref. [6].

structure. Apart from the resonant contribution, the shape of the tree-level distribution resembles the SM prediction (dashed black line), taking into account that $\kappa_\lambda^{(0)} < 1$.

Turning to the red line, incorporating one-loop corrections to both THCs, one can observe that the shape of the distribution changes drastically. In particular the cancellation close to the kinematical threshold in the leading order distribution is lifted. This cancellation now happens at values of $m_{hh} \approx 400$ GeV and leads to a large reduction of the differential cross section in the region where at leading order a maximum occurred. Furthermore, close to the kinematical threshold the distribution is largely enhanced, leading to the appearance of a structure resembling a peak at $m_{hh} \approx 250$ GeV.

Also shown in the figure are the total cross section values. The total cross section values are given at LO QCD in accordance with the distributions given at LO. Including the NLO QCD corrections obtained with `HPAIR`, the cross section values would increase by about a factor of 2 [21]. Here it is interesting to note that the decrease in the tree level value of κ_λ of about 15% w.r.t. the SM leads to an increase of roughly 20% of the tree level cross section, whereas the inclusion of the one-loop corrections to the THCs results in a reduction of the 2HDM cross section by about 30%, i.e. 20% smaller than the SM result.

The right plot of Fig. 2 shows the same m_{hh} distributions, but now we apply a smearing of 15% and a binning in m_{hh} of 50 GeV in order to take into account the limited detector resolution in the experimental analyses, see Ref. [21] for details. Again the distribution with the THCs at the tree level (blue line) largely resembles the SM m_{hh} distribution (black dashed). The effect of the resonance itself is very small, since its contribution to the full result is only about 4%. Furthermore, the "resonance-like" structure of the full result is caused dominantly by the contribution of the continuum diagrams, which peaks slightly above the di-top production threshold (~ 400 GeV), while the resonant contribution (at ~ 465 GeV) in this case is minor and does not appear as a clear

resonant structure above the continuum distribution. As can be inferred from the increase of $\lambda^{(1)}_{hhH}$ as compared to $\lambda^{(0)}_{hhH}$, the pure resonant contribution in this example is increased. As indicated by the red curve in the right plot, the combined effect of taking into account non-resonant contributions, interference effects and the NLO corrections to the THCs has a drastic effect on the predicted m_{hh} distribution. The resulting m_{hh} distribution is overall smoothly falling with just a small modulation near $m_{hh} \approx m_H$. Resolving this structure experimentally will clearly be very challenging. A striking feature that can be inferred from the plot is the large effect of the non-resonant contributions on the m_{hh} distribution just above the threshold at $m_{hh} \sim 250$ GeV. The shape of the differential cross section in this region is very significantly modified in comparison to the prediction using the THCs at lowest order (blue line). As discussed above, this enhancement happens as a result of a the change in κ_λ which affects the cancellation between the triangle and box form factors of the continuum diagrams that is present at the m_{hh} threshold at leading order. For $\kappa_\lambda \neq 1$ this cancellation does not take place, giving rise to a large enhancement just above the threshold, even after taking into account the 15% smearing and 50 GeV binning.

4. Impact of THC loop corrections on experimental limits

In view of the significant improvements in the experimental sensitivity to the di-Higgs production cross section that have occurred recently and are expected to be achieved in the future it is crucial that the experimental limits (and of course eventually also the experimental measurements) are presented in such a way that they can be confronted with theoretical predictions in different scenarios of electroweak symmetry breaking in a well-defined way. Up to now the experimental limits presented by ATLAS and CMS are given either for non-resonant production, taking into account only SM-like contributions, or for purely resonant production, where SM-like non-resonant contributions are omitted. We review the first type of limits, whereas a discussion of the latter can be found in Ref. [6].

In the case of non-resonant limits, they are obtained under the assumption that there is no contribution from an s-channel exchange of an additional Higgs boson, i.e. only the contributions of diagrams A and C in Fig. 1 are taken into account. The latest results from ATLAS [22][2] and CMS [24] report a limit on the cross section of $gg \to hh$, which depends on the value of κ_λ, and a bound on κ_λ is extracted. This is done by comparing the experimental limit with the SM prediction for a varied κ_λ. We show in Fig. 3 an example of the application of these limits for one particular benchmark scenario in the 2HDM, where we vary $c_{\beta-\alpha}$. The chosen input parameters are

$$\begin{aligned} t_\beta = 10,\ c_{\beta-\alpha} \in \{0 \ldots 0.16\}\ (s_{\beta-\alpha} > 0), \\ m_H = m_A = m_{H^\pm} = 1000\ \text{GeV},\ m_{12}^2 = m_H^2 c_\alpha^2 / t_\beta\ . \end{aligned} \tag{4.1}$$

The large m_H value ensures that the resonant contribution from the s-channel H exchange is negligible. The variation of $c_{\beta-\alpha}$ results in a variation of κ_λ as indicated in the left plot of Fig. 3. The blue dashed line shows the prediction for κ_λ at lowest order, while the blue solid line shows the one-loop prediction for κ_λ. The gray line indicates the value of $\kappa_\lambda = 1$, which corresponds to a coupling value of $\lambda_{hhh} = \lambda^{(0)}_{\rm SM}$. The parameter spaces that are excluded by theoretical constraints

[2]The most recent ATLAS result [23] shows slightly weaker limits, but has no qualitative effect on our results.

are indicated by the yellow (vacuum stability), dark green (perturbative unitarity at LO) and light green (perturbative unitarity at NLO) shaded areas. For the application of these limits we used the public package `thdmTools` [25]. The constraints from vacuum stability exclude the displayed yellow region with negative values of $c_{\beta-\alpha}$. For the largest positive values of $c_{\beta-\alpha}$ the tightest bound arises from perturbative unitarity. Demanding that the measured properties of the Higgs boson at 125 GeV should be satisfied poses a bound that is weaker than the one from NLO perturbative unitarity and therefore this bound is not explicitly shown in the plot. It can be observed that at tree level the variation of $c_{\beta-\alpha}$ towards larger values results in a decrease of $\kappa_\lambda^{(0)}$, which reaches values close to zero for $c_{\beta-\alpha} \gtrsim 0.1$. Including the one-loop corrections, as shown by the blue solid line, yields a strong increase of $\kappa_\lambda^{(1)}$, with $\kappa_\lambda^{(1)} \gtrsim 5$ for $c_{\beta-\alpha} \gtrsim 0.1$ in this example.

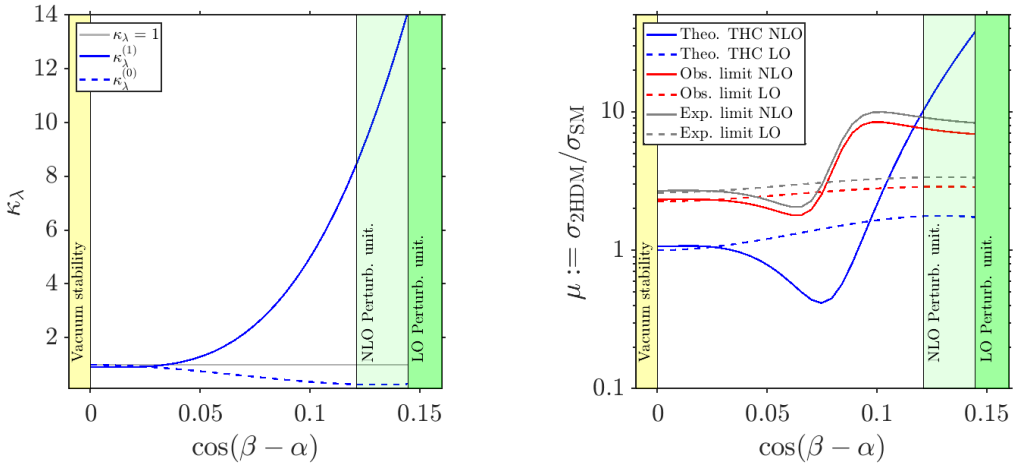

Figure 3: 2HDM type I scenario described in Eq. (4.1). Left: κ_λ as a function of $c_{\beta-\alpha}$. For the line styles: see text. Right: Limits on $\mu \equiv \sigma_{2HDM}/\sigma_{SM}$ (each cross section calculated at LO QCD) as function of $c_{\beta-\alpha}$. For the colored regions and line styles: see text. Plots taken from Ref. [6].

In the right plot we present the corresponding experimental limits and theoretical predictions for the ratio between the 2HDM and SM di-Higgs cross sections, $\mu \equiv \sigma_{2HDM}/\sigma_{SM}$, both calculated at LO QCD at $\sqrt{s} = 13$ TeV. The solid (dashed) blue line shows the theory prediction using the one-loop (tree-level) value for κ_λ. The red line shows the latest experimental observed limit from non-resonant searches reported by ATLAS [22] (see, however, Ref. [23]). The solid (dashed) line indicates the observed limit for the value of κ_λ which we have calculated at NLO (LO). The corresponding gray line represents the expected limit for κ_λ at NLO (LO). Confronting the experimental limits with the theoretical predictions, a value of $c_{\beta-\alpha}$ is regarded as excluded if the predicted cross section is larger than the experimentally excluded one. One can see that non-resonant di-Higgs searches would not exclude any value of $c_{\beta-\alpha}$ for the case where $\kappa_\lambda^{(0)}$ is used. As a consequence of the large loop corrections to κ_λ this changes once the one-loop corrections are taken into account. One can see that in this case for the considered example the non-resonant searches exclude a region for large $c_{\beta-\alpha}$ values that is allowed by all other constraints.

Acknowledgements

S.H. thanks the organizers of Loops & Legs 2024 for the invitation and the (as always!) inspiring atmosphere. The work of S.H. has received financial support from the grant PID2019-110058GB-C21 funded by MCIN/AEI/10.13039/501100011033 and by "ERDF A way of making Europe", and in part by the grant IFT Centro de Excelencia Severo Ochoa CEX2020-001007-S funded by MCIN/AEI/10.13039/501100011033. S.H. also acknowledges support from Grant PID2022-142545NB-C21 funded by MCIN/AEI/10.13039/501100011033/ FEDER, UE. The work of M.M. has been supported by the BMBF-Project 05H21VKCCA. K.R. and G.W. acknowledge support by the Deutsche Forschungsgemeinschaft (DFG, German Research Foundation) under Germany's Excellence Strategy – EXC 2121 "Quantum Universe" – 390833306. This work has been partially funded by the Deutsche Forschungsgemeinschaft (DFG, German Research Foundation) - 491245950.

References

[1] S. Kanemura, Y. Okada, E. Senaha and C. P. Yuan, Phys. Rev. D **70** (2004), 115002 [arXiv:hep-ph/0408364 [hep-ph]].

[2] S. Kanemura, Y. Okada and E. Senaha, Phys. Lett. B **606** (2005), 361-366 [arXiv:hep-ph/0411354 [hep-ph]].

[3] H. Bahl, J. Braathen and G. Weiglein, Phys. Rev. Lett. **129** (2022) no.23, 23 [arXiv:2202.03453 [hep-ph]].

[4] J. de Blas *et al.* JHEP **01** (2020), 139 [arXiv:1905.03764 [hep-ph]].

[5] [ATLAS], ATL-PHYS-PUB-2022-053.

[6] S. Heinemeyer, M. Mühlleitner, K. Radchenko and G. Weiglein, [arXiv:2403.14776 [hep-ph]].

[7] G. C. Branco *et al.*, Phys. Rept. **516** (2012), 1-102 [arXiv:1106.0034 [hep-ph]].

[8] S. Kanemura f*et al.*, Phys. Lett. B **558** (2003), 157-164 [arXiv:hep-ph/0211308 [hep-ph]].

[9] J. Braathen and S. Kanemura, Phys. Lett. B **796** (2019), 38-46 [arXiv:1903.05417 [hep-ph]].

[10] P. Basler and M. Mühlleitner, Comput. Phys. Commun. **237** (2019), 62-85 [arXiv:1803.02846 [hep-ph]].

[11] P. Basler, M. Mühlleitner and J. Müller, Comput. Phys. Commun. **269** (2021), 108124 [arXiv:2007.01725 [hep-ph]].

[12] P. Basler *et al.*, [arXiv:2404.19037 [hep-ph]].

[13] E. J. Weinberg, [arXiv:hep-th/0507214 [hep-th]].

[14] S. R. Coleman and E. J. Weinberg, Phys. Rev. D **7** (1973), 1888-1910.

[15] M. Mühlleitner, J. Schlenk and M. Spira, JHEP **10** (2022), 185 [arXiv:2207.02524 [hep-ph]].

[16] T. Plehn, M. Spira and P. M. Zerwas, Nucl. Phys. B **479** (1996), 46-64 [erratum: Nucl. Phys. B **531** (1998), 655-655] [arXiv:hep-ph/9603205 [hep-ph]].

[17] S. Dawson, S. Dittmaier and M. Spira, Phys. Rev. D **58** (1998), 115012 [arXiv:hep-ph/9805244 [hep-ph]].

[18] R. Gröber, M. Mühlleitner and M. Spira, Nucl. Phys. B **925** (2017), 1-27 [arXiv:1705.05314 [hep-ph]].

[19] H. Abouabid *et al.*, JHEP **09** (2022), 011 [arXiv:2112.12515 [hep-ph]].

[20] J. Baglio *et al.*, Eur. Phys. J. C **83** (2023) no.9, 826 [arXiv:2303.05409 [hep-ph]].

[21] F. Arco, S. Heinemeyer, M. Mühlleitner and K. Radchenko, Eur. Phys. J. C **83** (2023) no.11, 1019 [arXiv:2212.11242 [hep-ph]].

[22] G. Aad *et al.* [ATLAS], Phys. Lett. B **843** (2023), 137745 [arXiv:2211.01216 [hep-ex]].

[23] [ATLAS], ATLAS-CONF-2024-005.

[24] A. Tumasyan *et al.* [CMS], Nature **607** (2022) no.7917, 60-68 [erratum: Nature **623** (2023) no.7985, E4] [arXiv:2207.00043 [hep-ex]].

[25] T. Biekötter *et al.*, JHEP **01** (2024), 107 [arXiv:2309.17431 [hep-ph]].